Journal of the Serbian Chemical Society
JSCS-info@shd.org.rs • www.shd.org.rs/JSCS
J. Serb. Chem. Soc. *85* (11) 1475–1488 (2020)
JSCS–5388
UDC 546.47–31:66.017:544.526.5:613.28
Original scientific paper

Zinc oxide nanoparticles prepared by thermal decomposition of zinc benzenepolycarboxylato precursors: Photoluminescent, photocatalytic and antimicrobial properties

LIDIJA RADOVANOVIĆ[1*#], JELENA D. ZDRAVKOVIĆ[1], BOJANA SIMOVIĆ[2#], ŽELJKO RADOVANOVIĆ[1#], KATARINA MIHAJLOVSKI[3], MIROSLAV D. DRAMIĆANIN[4] and JELENA ROGAN[3#]

[1]Innovation Centre of Faculty of Technology and Metallurgy, University of Belgrade, Karnegijeva 4, Belgrade, Serbia, [2]Institute for Multidisciplinary Research, University of Belgrade, Kneza Višeslava 1, Belgrade, Serbia, [3]Faculty of Technology and Metallurgy, University of Belgrade, Karnegijeva 4, Belgrade, Serbia and [4]Vinča Institute of Nuclear Sciences, University of Belgrade, P. O. Box 522, Belgrade, Serbia

(Received 29 June, revised 14 August, accepted 17 August 2020)

Abstract: Zinc oxide (ZnO) nanoparticles were obtained by thermal decomposition of one-dimensional zinc–benzenepolycarboxylato complexes as single-source precursors at 450 °C in an air atmosphere. The mechanism and kinetics of thermal degradation of zinc–benzenepolycarboxylato complexes were analyzed under non-isothermal conditions in an air atmosphere. The results of X-ray powder diffraction and field emission scanning electron microscopy revealed hexagonal wurtzite structure of ZnO with an average crystallite size in the range of 39–47 nm and similar morphology. The band gap and the specific surface area of ZnO nanoparticles were determined using UV–Vis diffuse reflectance spectroscopy and the Brunauer, Emmett and Teller method, respectively. The photoluminescent, photocatalytic and antimicrobial properties of the ZnO nanoparticles were also examined. The best photocatalytic activity in the degradation of C. I. Reactive Orange 16 dye was observed for the ZnO powder where the crystallites form the smallest agglomerates. All ZnO nanoparticles showed excellent inhibitory effect against Gram-positive bacterium *Staphylococcus aureus* and Gram-negative bacterium *Escherichia coli*.

Keywords: nanomaterials; photoluminescence; photocatalysis; antimicrobial activity.

INTRODUCTION

Zinc oxide (ZnO) is a promising material due to its wide range of applications, as an ingredient in UV-protective coatings, solar cells, gas sensors as well

*Corresponding author E-mail: radovanovic@tmf.bg.ac.rs
[#] Serbian Chemical Society member.
https://doi.org/10.2298/JSC200629048R

as in degradation and mineralization of environmental pollutants.[1] It is nontoxic and biocompatible with excellent optical and electrical properties.[2,3] The versatile applications of ZnO gave as a result the expansion of numerous synthetic methods such as spray pyrolysis, sol–gel technique, solvo- and hydrothermal methods, atomic layer deposition, chemical precipitation, and thermal decomposition.[1] The synthetic techniques used for preparing ZnO nanoparticles have a tremendous impact to its properties,[1] and for this reason attention of researchers is oriented towards new and modification of known synthesis routes. The preparation methods have been intensively studied to control precisely the morphology of materials at the nanoscale. Thus, the synthesis of preferred ZnO nanomaterial usually requires templates, such as surfactants, that can import impurities, so additional post treatments need to be performed to obtain the pure product.[4] In recent years, the frequently used approach for the preparation of ZnO nanoparticles is based on the thermal decomposition of zinc coordination compounds in air in the temperature range from 160 to 900 °C during several hours.[4–8] This one-step method is simple, efficient, solvent and pollution free. It provides the possibility to control the size and shape of the obtain products by choosing the appropriate reaction conditions, such as the annealing temperature, reaction time, annealing rate as well as the precursor type and concentration.[4,9]

Mixed ligand complexes containing benzenpolycarboxylato (BPC) ligands are of special interest for the use as precursors in the synthesis of ZnO nanoparticles due to their different dimensionalities (from zero- to three-dimensional), which was found to be important for the size of the resulting oxide material. It has been shown that the oxide particles prepared by the thermolysis of three-dimensional complexes are larger than those obtained by the thermolysis of two- or one-dimensional complexes.[10,11] In addition, different synthetic conditions lead to ZnO nanoparticles of different morphologies (nanorods, nanotubes, flower-like nanoparticles, *etc*).[4] Therefore, the method of processing is important, because of the strong relationship between the size, morphology and properties of ZnO nanoparticles, such as photoluminescence,[12–14] photocatalytic[15–17] and antimicrobial activity.[18]

In this study, pure ZnO nanoparticles were prepared *via* the thermal decomposition of four previously obtained and structurally characterized one-dimensional Zn–BPC complexes with 2,2′-dipyridylamine (dipya): $[Zn(dipya)(pht)]_n$ (**1**, pht^{2-} is the dianion of 1,2-benzenedicarboxylic acid), $[Zn(dipya)(ipht)]_n$ (**2**, $ipht^{2-}$ is the dianion of 1,3-benzenedicarboxylic acid), $\{[Zn(dipya)(tpht)]\cdot H_2O\}_n$ (**3**, $tpht^{2-}$ is the dianion of 1,4-benzenedicarboxylic acid) and $[Zn_2(dipya)_2(pyr)]_n$ (**4**, pyr^{4-} is the tetraanion of 1,2,4,5-benzenetetracarboxylic acid).[19] Thermal analysis, as the most suitable method to study the thermal decomposition of complexes, was used to establish the optimal conditions for the thermal conversion of precursors to ZnO. In addition, the mechanism of thermal degradation of **1**–**4** was

studied under non-isothermal conditions in an air atmosphere. The kinetics of the solid-state reaction is of particular interest since it provides insights into processes occurring during solid-state reactions. The nanosized ZnO were characterized by X-ray powder diffraction (XRPD), field emission scanning electron microscopy (FESEM), the Brunauer, Emmett and Teller method (BET) and ultraviolet–visible diffuse reflectance spectroscopy (UV–Vis), and they were tested for their photoluminescent (PL), photocatalytic and antimicrobial properties.

EXPERIMENTAL

Solid-state synthesis of nanosized ZnO

Nanosized powders of ZnO_1, ZnO_2, ZnO_3 and ZnO_4 were obtained by the thermal degradation of precursors **1**–**4**, respectively. First, 2.0 g of each precursor was heated at the constant rate up to 450 °C, then, isothermally calcinated at 450 °C during 1 h, and finally, spontaneously cooled to room temperature.

Instruments and measurements

Thermogravimetric data for precursors **1**–**4** were collected on an SDT Q600 instrument (TA Instruments) for the simultaneous TGA-DTA/DSC analysis from room temperature to 650 °C, in air atmosphere (flow rate: 100 mL min^{-1}, sample masses ≈8 mg) at different heating rates (15, 20, 25 and 30 °C min^{-1}). The calibration of the instrument was performed for each heating rate separately. The details about solid-state kinetics under non-isothermal conditions are given in Supplementary Material to this paper. The XRPD data for ZnO powders were collected over the $20° < 2\theta < 75°$ range on an Ital Structures APD2000 X-ray diffractometer using Cu$K\alpha$ radiation (λ = 1.5418 Å), with the step size of 0.02° and a counting time of 1 s $step^{-1}$. The average crystallite size (<*D*>) of ZnO powders was calculated using the Scherrer formula.[20] An FESEM Tescan Mira 3 XMU was used for the morphological characterization of ZnO powders. Using Mira software, the micrographs were analyzed and the average diameters of the particles (more than 100 particles) were determined. The specific surface area (*SSA*) of ZnO powders was calculated according to the BET method from the linear part of the nitrogen adsorption isotherm at 77 K[21] on a Micrometrics ASAP 2020 instrument. Before the measurements, the samples were out-gassed at 150 °C for 10 h under vacuum. Diffuse reflectance UV–Vis spectra of the ZnO powders were recorded over the 200–800 nm spectral region ($BaSO_4$ was used as a reference standard) using a Shimadzu UV-2600 spectrophotometer equipped with an integrating sphere. PL measurements of ZnO powders were performed at room temperature on a Fluorolog-3 model FL3-221 spectrofluorimeter system (Horiba Jobin Yvon), utilizing a 450 W Xenon lamp as the excitation source for the steady-state measurements and a xenon–mercury pulsed lamp for the time-resolved measurements. The emission spectra of ZnO powders were scanned in the wavelength range from 350 to 600 nm and from 480 to 650 nm under 320 and 350 nm excitations, respectively. A TBX-04-D PMT detector was used for both the time-resolved and steady state acquisitions. The line intensities and positions of the measured spectra were calibrated with a standard Mercury–Argon lamp. The PL measurements were performed on pellets prepared from the powders under a load of 5000 kg.

Photocatalytic experiments

Photodegradation experiments using ZnO powders were performed using an open reactor (100 mL) in a dark chamber equipped with an Osram Ultra-Vitalux 300 W lamp, which, according to the specification, produces the radiation similar to natural sunlight. The intensity

of the lamp radiation was measured using a Voltcraft PL-110SM solar radiation measuring instrument and found to be 300 W m^{-2}. The lamp was placed 35 cm away from the surface of the dye solution. Constant mixing and temperature (20 °C) of the solution were maintained during the experiment. The photodegradation of C. I. Reactive Orange 16 dye (RO16) was studied by mixing 50 mL of an aqueous solution containing the dye (50 mg mL^{-1}) and ZnO catalyst (100 mg). The homogenous suspension was left in the dark for 30 min to achieve adsorption equilibrium. Subsequently, the lamp was switched on and after every 15 min of irradiation, the solution (3 mL) was sampled. The residual concentration of dye was determined using a UV–Vis spectrophotometer (Shimadzu 2600) after separation of the solution using a Whatman 0.45 μm membrane filter. The absorption spectra and rate of photodegradation were observed in terms of the absorbance change at the peak maximum of the dye (λ_{max} = = 492.5 nm). Commercial ZnO (MKN-ZnO-020, mkNano, Mississauga, ON, USA) was treated in the same way. The kinetics parameters, reaction rate constant (k, min^{-1}) and correlation coefficient (R^2), for the photocatalytic removal of RO16 were calculated by fitting assuming pseudo-first kinetic order of the reaction:

$$\ln (c_0/c) = k\tau \quad (1)$$

where c_0 is the initial concentration of the dye (mg L^{-1}), c is the concentration (mg L^{-1}) at any time, τ (min).

Antimicrobial test

Quantitative tests of the antimicrobial activity of all obtained ZnO powders against Gram-positive (G^+) bacterium *Staphylococcus aureus* (ATCC 25923), Gram-negative (G^-) bacterium *Escherichia coli* (ATCC 25922) and yeast *Candida albicans* (ATCC 10259) were performed according to the liquid challenge method in sterile normal saline solution. A mass of 0.01 g of each ZnO powder was suspended in a tube containing 0.9 mL of sterile normal saline and inoculated with 0.9 mL bacterial suspension to achieve a concentration of $1 \cdot 10^5$ cfu cm^{-1}. The tubes were then incubated at 37 °C for 1 h. After incubation, 9 mL of sterile normal saline was added. Subsequently, 1 mL aliquots were taken as samples for viable cell determination. Sterile normal saline solution was used for dilution of the number of colonies and 0.1 mL of the appropriately diluted solution was placed in a Petri dish and overlaid with TSAY (Tripton soy agar with 0.6 % yeast extract). The Petri dishes were incubated at 37 °C for 24 h. As a control, a blank sterile normal saline solution without sample was used. The degree of reduction, R (%), was calculated according to:

$$R = 100(CFU_{cont} - CFU_M)/CFU_{cont} \quad (2)$$

where CFU_{cont} is the number of microorganism colonies in the control tube and CFU_M is the number of microorganism colonies in the tubes with the samples. All analyses of the antimicrobial activity determination were run in triplicate and the mean value and standard deviation were calculated.

RESULTS AND DISCUSSION

*Mechanism, thermodynamics and kinetics of thermal degradation of precursors **1**–**4***

In air atmosphere, complexes **1**–**4** decompose in two (**4**), three (**1** and **2**) or four (**3**) steps (Fig. 1). The TG curves of **1**, **2** and **4** show stability under 350 °C, indicating the absence of water molecules and other adsorptive solvent molecules. Multistep decomposition of **1**–**4** results in ZnO formation up to 560 °C

(found 19.0 %; calc. 20.3 % for **1**; found 21.4 %; calc. 20.3 % for **2**; found 17.2 %; calc. 19.4 % for **3** and found 22.5 %; calc. 21.5 % for **4**). The decomposition pathway of each precursor is proposed, within the corresponding temperature ranges (Table S-I of the Supplementary material). The decomposition of **1**, **2** and **4** (Fig. 1) manifested itself as an endothermic effect in the corresponding DSC curves (the peak maxima: 369 °C for **1**, 410 °C for **2** and 421 °C for **4**), while the total combustion of organic ligand and carbon deflagration is verified by an exothermic one (the peak maxima located: 509 °C for **1**, 510 °C for **2** and 511 °C for **4**). For **3**, thermal degradation starts with dehydration that is accompanied with endothermic DSC peak with a maximum located around 156 °C, while the other two degradation steps are also determined as endothermic processes with maxima placed about 315 and 396 °C (Fig. 1).

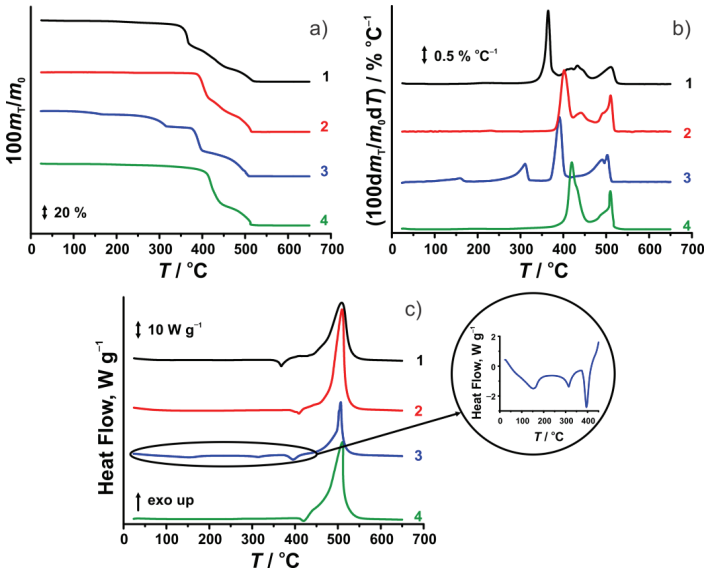

Fig. 1. TG (a), DTG (b) and DSC (c) curves of **1**–**4** at β = 20 °C min^{-1} in an air atmosphere.

The fourth peak in the DSC curve of **3** is exothermic with peak maxima at 507 °C due to complete combustion of the residual organic fragments. The degradation of **1** and **4** starts with dipya release (Table S-I), due to greater Zn–O bond strength compared to that of the Zn–N bond, which was in accordance with a previous study concerning the higher bond strength of transition metal ions with monodentately coordinated O atoms than those with N atoms.[22–24] The thermal decompositions of **2** and **3** are different compared to those of **1** and **4**. In **2**, the Zn–O bonds between the Zn and O atom from one chelately coordinated COO^- group are weaker in comparison to the Zn–N bonds, meaning that the degradation of this precursor starts with the loss of part of the ipht ligand.[19,25] The

degradation of anhydrous precursor **3** can be described in a similar way, beginning with loss of part of the tpht ligand (Table S-I).

The kinetic parameters, especially E_a and $\Delta S^{\#}$, are helpful in assigning the strength of the bonding of ligands with metal ions. The values presented in Table S-II of the Supplementary material are well within limits found for the degradation of transition metal complexes and inorganic salts.[26] By comparing the apparent energies of activation, it could be concluded that the thermal stability of the complexes decreases in the order: **4** > **2** > **1** > **3**. The negative values of $\Delta S^{\#}$ indicate that the activated complexes were less disordered than the reactants, as was found for similar Ni(II)–BPC complexes with N donor ligands.[27] Thus, the decomposition processes of the precursors **1**–**4** may be compared based on the values of $\Delta S^{\#}$; a value of $\Delta S^{\#}$ is less negative for an easier decomposition process, which was proven in the case of precursor **3**. The main aim of the thermal analysis and solid-state kinetics was to investigate the thermal stability and decomposition mechanism of **1**–**4**. Thermal analysis and solid-state kinetics were performed under non-isothermal conditions, while the ZnO nanoparticles were prepared under isothermal conditions by calcination of **1**–**4** at 450 °C. This temperature was chosen as the lowest temperature for complete degradation of **1**–**4**, as well as to avoid the increase of crystallite size of the obtained ZnO nanoparticles.[6,8]

Characterization of ZnO nanoparticles

The thermolysis of the complexes **1**–**4** resulted in the oxides ZnO_1, ZnO_2, ZnO_3 and ZnO_4, respectively, and their XRPD patterns are shown in Fig. S-1 of the Supplementary material. The patterns confirmed that the final product of solid-state thermolysis of all precursors was ZnO, which crystallizes in the hexagonal wurtzite structure with a $P6_3mc$ space group (PDF # 80-0074). The unit cell parameters and the calculated values of <*D*> for the obtained ZnO_1–ZnO_4 oxides, together with corresponding values for commercial ZnO powder (ZnO_com) are listed in Table I. As can be seen, the unit cell of the prepared ZnO_1–ZnO_4 powders is slightly smaller than the unit cell of ZnO_com, while the value of <*D*> is about two times bigger.

TABLE I. The unit cell parameters, <*D*>, *SSA* and E_g of ZnO_1–ZnO_4 and ZnO_com

Sample	*a* / Å	*c* / Å	*V* / Å^3	<*D*> / nm	*SSA*, m^2 g^{-1}	E_g / eV
ZnO_1	3.2528(1)	5.2142(2)	47.779(4)	39(1)	7.4	3.14
ZnO_2	3.2539(1)	5.2074(2)	47.749(4)	47(1)	5.8	3.15
ZnO_3	3.2528(1)	5.2142(2)	47.779(4)	44(1)	7.7	3.22
ZnO_4	3.2522(1)	5.2131(2)	47.752(4)	44(1)	7.5	3.13
ZnO_com	3.2520(1)[28]	5.2178(2)[28]	47.788(3)[28]	22(1)[28]	46.3	3.12

The results of the FESEM analysis of ZnO powders are presented in Fig. 2.

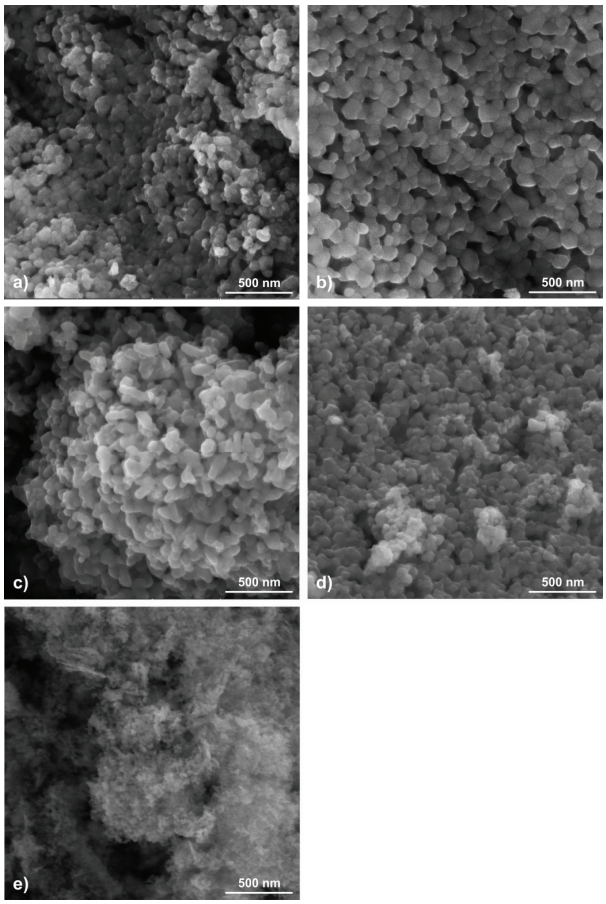

Fig. 2. FESEM images of nanoparticles of ZnO_1 (a), ZnO_2 (b), ZnO_3 (c), ZnO_4 (d) and ZnO_com (e).

Slightly elongated particles were observed for ZnO_3, while the morphologies of ZnO_1, ZnO_2, ZnO_4 and ZnO_com were very similar consisting of nanoparticles with approximately spherical or rounded hexagonal shapes. In addition, it was revealed that the morphologies of the starting precursors **1**–**4** (Fig. S-2 of the Supplementary material) after calcination are not maintained in ZnO_1–ZnO_4, probably due to high annealing rate (about 20 °C min^{-1}). The estimated particle size was about 55, 78, 75, 56 and 28 nm for ZnO_1–ZnO_4 and ZnO_com, respectively. Nevertheless, the nanoparticles of each powder form agglomerates with different average size of about 2.26(±1.23) μm for ZnO_1, 8.02(±3.23) μm for ZnO_2, 1.25(±0.37) μm for ZnO_3, 3.56(±1.94) μm for ZnO_4 and 2.64(±1.15) μm for ZnO_com (Fig. S-3 of the Supplementary material). BET measurements showed that the *SSA* values of the ZnO_1–ZnO_4

nanoparticles were in the range of 5.8–7.7 m^2 g^{-1} (Table I), and these values are significantly smaller than the value estimated for ZnO_com (46.3 m^2 g^{-1}), which is in accordance with notably smaller crystallite size for ZnO_com. The values of the band gap energy (E_g) of ZnO_1–ZnO_4 and ZnO_com (Table I) were calculated from a plot of the modified Kubelka–Munk function $(F(R)hv)^2$ *vs.* the energy of the adsorbed light (hv) using linear fits close to the absorption edge, as is shown in Fig. S-4 of the Supplementary material, and obtained results are in accordance with literature data for pure ZnO.[29]

Photoluminescent properties of ZnO nanoparticles

Steady-state emission spectra of ZnO_1–ZnO_4 and ZnO_com obtained at room temperature are shown in Fig. 3. Upon excitation at 320 nm, the emission shows the maximum value in the UV spectral region at 379 (ZnO_1), 380 (ZnO_2), 379 (ZnO_3), 384 (ZnO_4) and 393 nm (ZnO_com). These values are in good agreement with the determined band gap values for each sample (Table I). The highest intensity of PL was observed for ZnO_4 (five times higher than ZnO_3), and the emission intensity decreases in the order ZnO_4 > ZnO_3 > ZnO_com > ZnO_1 > ZnO_2. The intense ZnO_4 emission may be associated with the crystal structure having fewer defects than the other investigated oxides.[30]

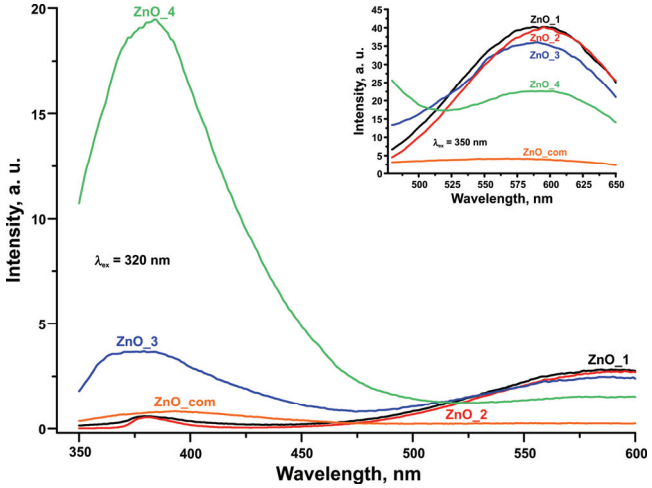

Fig. 3. Emission spectra of ZnO_1–ZnO_4 and ZnO_com in UV and visible (inset) spectral regions.

To determine the emission maxima in the visible region, the PL of the oxide samples were additionally measured upon excitation at 350 nm (Fig. 3, inset). It was observed that the emission maxima were at 595, 595, 591, 593 and 566 nm for ZnO_1–ZnO_4 and ZnO_com, respectively. The evaluated emission maxima are in the yellow area of the visible spectrum, which is most often associated with

defects in the structure.[31–33] The most intense emission in the yellow region was observed for ZnO_1 and ZnO_2, while the PL of ZnO_com was negligible in this area. The better PL properties of ZnO_1 and ZnO_2 in the visible region are probably due to large number of defects compared to the other examined samples.

Photocatalytic properties of ZnO nanoparticles

To evaluate the photocatalytic performance of ZnO_1–ZnO_4 and ZnO_com, the dependence of RO16 concentration on irradiation time was measured and the results presented in Fig. 4. All the investigated samples showed a notable degradation confirming that these powders are active photocatalysts for RO16. The oxide samples exhibited different behaviors during the adsorption and photocatalytic degradation. ZnO_com shows the best adsorption power by adsorbing around 20 % of the dye from the solution, while a lower adsorption was identified for the ZnO_4 surface with the less than 10 % of the dye adsorbed during 30 min in the dark (Fig. 4). The strong adsorption power of ZnO_com is related to a notably higher *SSA* in comparison to the almost seven times lower values of *SSA* for ZnO_1–ZnO_4 (Table I). However, the photocatalytic efficiency decreases in the following order: ZnO_3 > ZnO_1 ≈ ZnO_com ≈ ZnO_2 ≈ ZnO_4. The higher photocatalytic activity of ZnO_3 was demonstrated by complete degradation of RO16 15 min earlier in comparison to the other samples, which could be explained by the fact that the ZnO_3 particles form the smallest agglomerates (Fig. S-3). The problem of particle agglomeration, together with considerations about agglomerate size is often discussed in studies dealing with adsorption properties of ZnO nanoparticles.[1,34] The agglomeration could cause negative effects, such as light blocking by large agglomerates and the decrease of active surface of the catalyst, all of which reduce the ability of the catalyst to produce the radicals necessary for the degradation of the dye.[1,34]

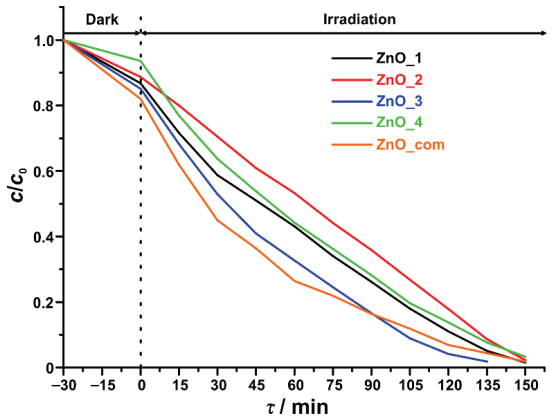

Fig. 4. The rate of photodegradation of RO16 dye in aqueous suspensions of ZnO_1–ZnO_4 and ZnO_com.

Plots of $\ln(c_0/c)$ of RO16 *vs*. irradiation time for the photocatalytic degradation of RO16 on the investigated ZnO powders are shown in Fig. S-5 of the Supplementary material. The values of R^2 for the fitted line were in the range from 0.80 to 0.95 (Table II), confirming the pseudo-first order model to describe the kinetics of RO16 degradation. Generally, the pseudo-first kinetic order is correct for concentrations up to 60 mg L^{-1} and many studies were well fitted by this model.[28,35] The decreasing order of the k values was compatible with the decreasing order of the photocatalytic efficiency of the powders (Table II).

TABLE II. The values of k and R^2 for ZnO_1–ZnO_4 and ZnO_com

Sample	k / min^{-1}	R^2
ZnO_1	0.0233	0.86
ZnO_2	0.0202	0.80
ZnO_3	0.0267	0.92
ZnO_4	0.0200	0.91
ZnO_com	0.0229	0.95

Antimicrobial activity of ZnO nanoparticles

Antibacterial and antifungal activities of ZnO_1–ZnO_4 and ZnO_com were examined on *Staphylococcus aureus* (G^+ bacterium), *Escherichia coli* (G^- bacterium), and yeast *Candida albicans* and the results are presented in Table III. All examined samples showed excellent inhibitory effects against the tested bacteria, while a decrease in the growth of *C. albicans* was not observed. The mechanism for the antibacterial activity of ZnO is still under consideration and there are some possible explanations for the toxicity of ZnO towards bacteria: a) Zn^{2+} from the ZnO nanoparticles may enter into the bacteria and cause disturbances of its amino acid metabolism, enzyme systems and the transport of substances, leading eventually to death of bacteria;[18] b) antibacterial activity is most stimulated with the production of reactive oxygen species (ROS), such as OH^-, O^{2-} and H_2O_2, from the ZnO surface. The first two species damage the surface of the bacteria, while H_2O_2 can enter into the bacteria causing their death;[18] c) the antibacterial effect of ZnO could be connected with the abrasive surface texture of ZnO due to surface defects;[36] d) an increase in the concentration of ZnO leads to better antibacterial activity.[18] It could be assumed that the production of ROS from the surfaces of the investigated ZnO was probably the main mechanism for growth inhibition of the tested bacteria. Excellent antibacterial activities of ZnO_1–ZnO_3 could be connected with the existence of defects in their crystal structures, observed by PL measurements. In contrast to bacteria, yeast exhibits a higher stability towards ZnO due to a different cell structure than bacteria, as well as due to higher resistance to ROS.[37] The poor antifungal activity of ZnO nanoparticles in this study is presumably related to the formation of the agglomerates of relatively large dimensions, which is consistent with previous findings.[38]

TABLE III. Data for the antimicrobial test of ZnO_1–ZnO_4 and ZnO_com; n. a. = not active

Sample	Number of colonies and *R* / %					
	Staphylococcus aureus		*Escherichia coli*		*Candida albicans*	
	No. of colonies	*R* / %	No. of colonies	*R* / %	No. of colonies	*R* / %
Control	$4.38 \cdot 10^7$	–	$8.20 \cdot 10^6$	–	$4.65 \cdot 10^5$	–
ZnO_1	–	100	–	100	$1.07 \cdot 10^6$	n. a.
ZnO_2	–	100	–	100	$1.83 \cdot 10^6$	n. a.
ZnO_3	–	100	–	100	$2.37 \cdot 10^6$	n. a.
ZnO_4	–	100	–	100	$2.02 \cdot 10^6$	n. a.
ZnO_com	$1.60 \cdot 10^2$	99.85±0.07	–	100	$7.49 \cdot 10^5$	n. a.

CONCLUSIONS

ZnO nanoparticles (ZnO_1, ZnO_2, ZnO_3 and ZnO_4), with hexagonal wurtzite structure and an average crystallite size of 39–47 nm, were prepared by the thermal decomposition of Zn–benzenepolycarboxylato precursors. The results of the mechanism and kinetics study showed the highest thermal stability of precursor **4**. FESEM analyses revealed that morphologies of ZnO nanoparticles are slightly elongated (ZnO_3) and approximately hexagonal (ZnO_1, ZnO_2 and ZnO_4), whereas the agglomeration of nanoparticles is significant. The values of *SSA* determined using the BET method were small, ranging from 5.8 to 7.7 $m^2 g^{-1}$. PL measurements showed that UV emission was dominant in the emission spectra of ZnO_4, while the visible emission was stronger in the case of ZnO_1 and ZnO_2. All the obtained ZnO nanoparticles were used as photocatalysts in the degradation of RO16 dye, whereby ZnO_3 showed the highest photocatalytic performance by degrading the dye in 135 min under illumination similar to natural sunlight. All oxides displayed excellent antibacterial activities against *S. aureus* and *E. coli*.

SUPPLEMENTARY MATERIAL

Details about the solid-state kinetics under non-isothermal conditions, thermogravimetric results for **1**–**4**, thermodynamic and kinetic parameters of the thermal degradation of **1**–**4**, FESEM images of **1**–**4**, XRPD patterns and FESEM images of ZnO nanoparticles, $(F(R)hv)^2$ *vs. hv* plots and linear plots of pseudo-first order kinetic model of RO16 degradation on ZnO nanoparticles are available electronically from http://www.shd.org.rs/JSCS/, or from the corresponding author on request.

Acknowledgements. We are indebted to Dr. Ivana Zeković from Vinča Institute of Nuclear Sciences, University of Belgrade, for her help with the photoluminescence measurements. This work was supported by the Ministry of Education, Science and Technological Development of the Republic of Serbia (Contract No. 451-03-68/2020-14/200287 and Contract No. 451-03-68/2020-14/200135).

ИЗВОД

НАНОЧЕСТИЧНИ ПРАХОВИ ЦИНК-ОКСИДА ДОБИЈЕНИ ТЕРМИЧКОМ ДЕГРАДАЦИЈОМ ЦИНК-БЕНЗЕНПОЛИКАРБОКСИЛАТО ПРЕКУРСОРА: ФОТОЛУМИНЕСЦЕНТНА, ФОТОКАТАЛИТИЧКА И АНТИМИКРОБНА СВОЈСТВА

ЛИДИЈА РАДОВАНОВИЋ[1*], ЈЕЛЕНА Д. ЗДРАВКОВИЋ[1], БОЈАНА СИМОВИЋ[2], ЖЕЉКО РАДОВАНОВИЋ[1], КАТАРИНА МИХАЈЛОВСКИ[3], МИРОСЛАВ Д. ДРАМИЋАНИН[4] и ЈЕЛЕНА РОГАН[3]

[1]*Иновациони центар Технолошко–металуршког факултета, Универзитет у Београду, Карнегијева 4, Београд,* [2]*Институт за мултидисциплинарна истраживања, Универзитет у Београду, Кнеза Вишеслава 1, Београд,* [3]*Технолошко–металуршки факултет, Универзитет у Београду, Карнегијева 4, Београд и* [4]*Институт за нуклеарне науке „Винча", Универзитет у Београду, п. пр. 522, Београд*

Термичком деградацијом једнодимензионалних цинк-бензенполикарбоксилато комплекса као прекурсора на 450 °C у оксидационој атмосфери добијени су наночестични цинк-оксиди (ZnO). Механизам и кинетика термичке разградње цинк-бензенполикарбоксилато комплекса анализирани су у неизотермским условима у атмосфери ваздуха. Рендгенском дифракцијом праха и скенирајућом електронском микроскопијом утврђена је хексагонална вурцитна структура ZnO са просечном величином кристалита у опсегу 39–47 nm и сличном морфологијом. Ширина забрањене зоне и специфична површина наночестичнх прахова ZnO одређени су ултраљубичастом–видљивом дифузно-рефлексионом спектроскопијом, односно БЕТ методом. Испитана су фотолуминесцентна, фотокаталитичка и антимикробна својства наночестица ZnO. Најбоља фотокаталитичка активност при разградњи боје C. I. Reactive Orange 16 уочена је код ZnO чији кристалити формирају најмање агломерате. Сви оксиди показали су одлично инхибиторско дејство на бактерије *Staphylococcus aureus* и *Escherichia coli*.

(Примљено 29. јуна, ревидирано 14. августа, прихваћено 17. августа 2020)

REFERENCES

1. A. Kołodziejczak-Radzimska, T. Jesionowski, *Materials* **7** (2014) 2833 (https://doi.org/10.3390/ma7042833)
2. A. Moezzi, A. M. McDonagh, M. E. Cortie, *Chem. Eng. J.* **185**/**186** (2012) 1 (https://doi.org/10.1016/j.cej.2012.01.076)
3. Z. L. Wang, *J. Phys.: Condens. Matter* **16** (2004) R829 (https://doi.org/10.1088/0953-8984/16/25/R01)
4. Y. Song, X. Li, L. Sun, L. Wang, *RSC Adv.* **5** (2015) 7267 (https://doi.org/10.1039/C4RA12273A)
5. J. Ban, G. Xu, L. Zhang, H. Lin, Z. Sun, Y. Lv, D. Jia, *J. Solid State Chem.* **256** (2017) 151 (http://dx.doi.org/10.1016/j.jssc.2017.09.002)
6. M. I. Khalil, M. M. Al-Qunaibit, A. M. Al-zahem, J. P. Labis, *Arab. J. Chem.* **7** (2014) 1178 (https://doi.org/10.1016/j.arabjc.2013.10.025)
7. H. Y. Shi, B. Deng, S. L. Zhong, L. Wang, A. W. Xu, *J. Mater. Chem.* **21** (2011) 12309 (https://doi.org/10.1039/C1JM10809C)
8. Y. Guo, R. Weiss, R. Boese, M. Epple, *Thermochim. Acta* **446** (2006) 101 (https://doi.org/10.1016/j.tca.2006.01.002)
9. R. R. Salunkhe, Y. V. Kaneti, Y. Yamauchi, *ACS Nano* **11** (2017) 5293 (https://doi.org/10.1021/acsnano.7b02796)
10. R. Das, P. Pachfule, R. Banerjee, P. Poddar, *Nanoscale* **4** (2012) 591 (https://doi.org/10.1039/C1NR10944H)
11. R. Kruszynski, M. Swiatkowski, *J. Saudi Chem. Soc.* **22** (2018) 816 (https://doi.org/10.1016/j.jscs.2018.01.003)

12. Y. Gong, T. Andelman, G. F. Neumark, S. O'Brien, I. L. Kuskovsky, *Nanoscale Res. Lett.* **2** (2007) 297 (https://doi.org/10.1007/s11671-007-9064-6)
13. S. Venkataprasad Bhat, S. R. C. Vivekchand, A. Govindaraj, C. N. R. Rao, *Solid State Commun.* **149** (2009) 510 (https://doi.org/10.1016/j.ssc.2009.01.014)
14. G. Xiong, U. Pal, J. Garcia Serrano, *J. Appl. Phys.* **101** (2007) 024317 (http://dx.doi.org/10.1063/1.2424538)
15. J. S. Chang, J. Strunk, M. N. Chonga, P. E. Poh, J. D. Ocon, *J. Hazard. Mater.* **381** (2020) 120958 (https://doi.org/10.1016/j.jhazmat.2019.120958)
16. D. Li, H. Haneda, *Chemosphere* **51** (2003) 129 (https://doi.org/10.1016/S0045-6535(02)00787-7)
17. A. C. Dodd, A. J. McKinley, M. Saunders, T. Tsuzuki, *J. Nanopart. Res.* **8** (2006) 43 (https://doi.org/10.1007/s11051-005-5131-z)
18. A. Sirelkhatim, S. Mahmud, A. Seeni, N. H. M. Kaus, L. C. Ann, S. K. M. Bakhori, H. Hasan, D. Mohamad, *Nano-Micro Lett.* **7** (2015) 219 (https://doi.org/10.1007/s40820-015-0040-x)
19. L. Radovanović, J. Rogan, D. Poleti, M. Milutinović, M. V. Rodić, *Polyhedron* **112** (2016) 18 (https://doi.org/10.1016/j.poly.2016.03.054)
20. H. P. Klug, L. E. Alexander, *X-ray diffraction procedures*, 2nd ed., Wiley, New York, 1974
21. F. Rouquerol, J. Rouquerol, K. Sing, *Adsorption by powders and porous solids*, Academic Press, London, 1999
22. J. Rogan, D. Poleti, *Thermochim. Acta* **413** (2004) 227 (https://doi.org/10.1016/j.tca.2003.10.015)
23. J. Rogan, D. Poleti, Lj. Karanović, Z. Jagličić, *J. Mol. Struct.* **985** (2011) 371 (https://doi.org/10.1016/j.molstruc.2010.11.024)
24. A. M. Abdalla, *J. Anal. Appl. Pyrolysis* **70** (2003) 687 (https://doi.org/10.1016/S0165-2370(03)00040-8)
25. J. D. Zdravković, L. Radovanović, D. Poleti, J. Rogan, P. Vulić, Ž. Radovanović, D. M. Minić, *Solid State Sci.* **80** (2018) 123 (https://doi.org/10.1016/j.solidstatesciences.2018.04.013)
26. C. H. Bamford, C. F. H. Tipper, *Compr. Chem. Kin.* **22** (1980) 115 (https://doi.org/10.1016/S0069-8040(08)70385-6)
27. J. Zdravković, D. Poleti, J. Rogan, N. N. Begović, V. A. Blagojević, M. Vasić, D. M. Minić, *J. Therm. Anal. Calorim.* **123** (2016) 1715 (https://doi.org/10.1007/s10973-015-5007-0)
28. B. Simović, D. Poleti, A. Golubović, A. Matković, M. Šćepanović, B. Babić, G. Branković, *Process. Appl. Ceram.* **11** (2017) 27 (https://doi.org/10.2298/PAC1701027S)
29. K. G. Chandrappa, T. V. Venkatesha, *Nano-Micro Lett.* **4** (2012) 14 (https://doi.org/10.1007/BF03353686)
30. D. Thapa, J. Huso, J. L. Morrison, C. D. Corolewski, M. D. McCluskey, L. Bergman, *Opt. Mater.* **58** (2016) 382 (https://doi.org/10.1016/j.optmat.2016.05.008)
31. S. A. Studenikin, N. Golego, M. Cocivera, *J. Appl. Phys.* **84** (1998) 2287 (https://doi.org/10.1063/1.368295)
32. Y. Ni, X. Wei, J. Hong, Y. Ye, *Mater. Sci. Eng., B* **121** (2005) 42 (https://doi.org/10.1016/j.mseb.2005.02.065)
33. A. B. Djurišić, Y. H. Leung, K. H. Tam, L. Ding, W. K. Ge, H. Y. Chen, S. Gwo, *Appl. Phys. Lett.* **88** (2006) 103107 (https://doi.org/10.1063/1.2182096)
34. F. Pellegrino, L. Pellutiè, F. Sordello, C. Minero, E. Ortel, V. D. Hodoroaba, V. Maurino, *Appl. Catal., B-Environ.* **216** (2017) 80 (https://doi.org/10.1016/j.apcatb.2017.05.046)

35. K. K. Ioannis, A. A. Triantafyllos, *Appl. Catal., B-Environ.* **49** (2004) 1 (https://doi.org/10.1016/j.apcatb.2003.11.010)
36. N. Padmavathy, R. Vijayaraghavan, *Sci. Technol. Adv. Mat.* **9** (2008) 035004 (https://doi.org/10.1088/1468-6996/9/3/035004)
37. R. Dobrucka, J. Dlugaszewska, M. Kaczmarek, *Biomed. Microdevices* (2018) 20 (https://doi.org/10.1007/s10544-017-0233-9)
38. O. Yamamoto, *Int. J. Inorg. Mater.* **3** (2001) 643 (https://doi.org/10.1016/S1466-6049(01)00197-0).